Supplemental Information

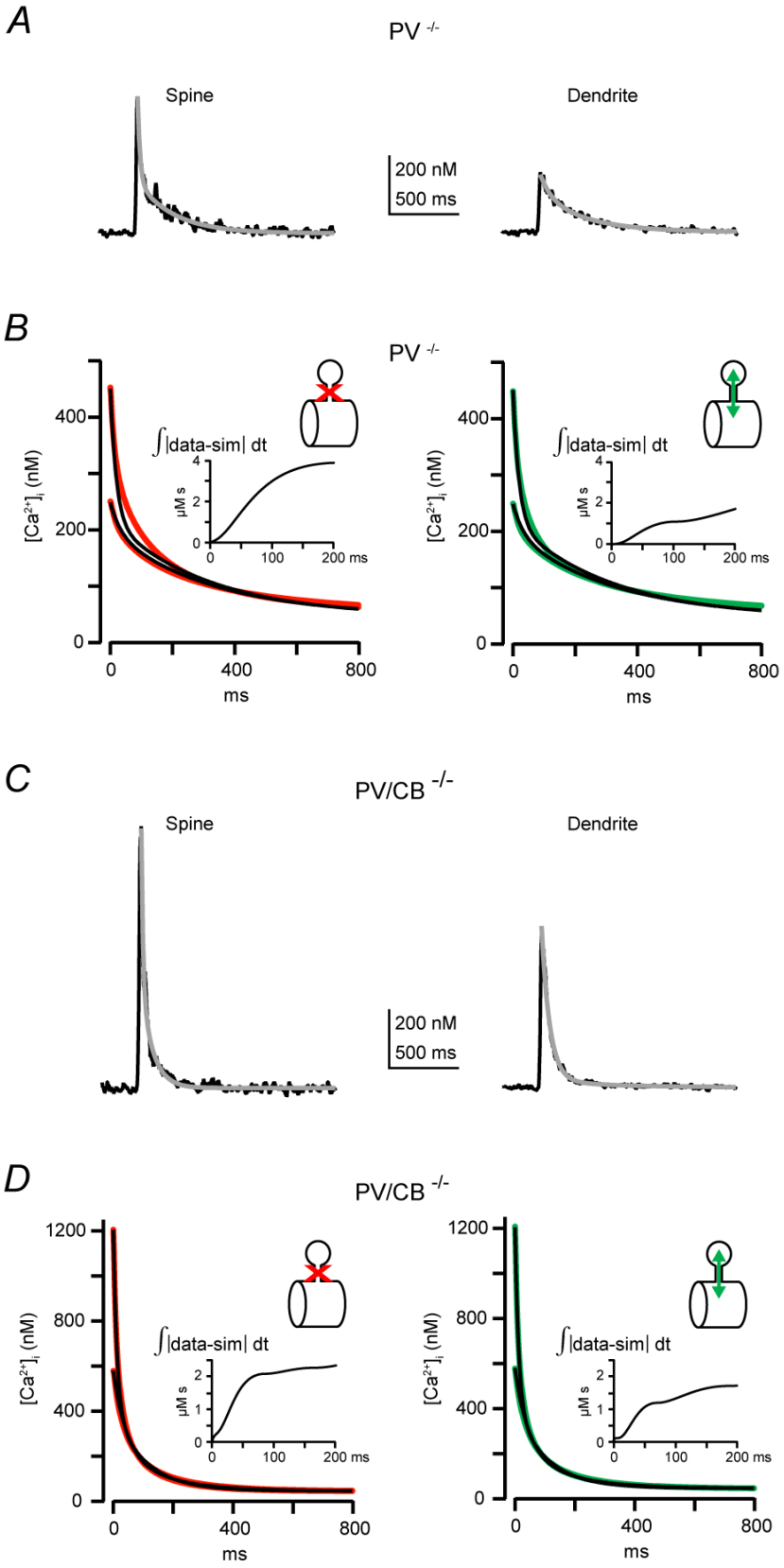

Supp. Fig. 1. Ca^{2+} kinetics in $PV^{-/-}$ and $PV/CB^{-/-}$ mice confirm predictions of the model

A, Ca^{2+} transients from a spine and the adjacent dendrite of a parvalbumin deficient ($PV^{-/-}$) PN (black lines) recorded under conditions identical to those described in Fig. 1. The grey lines represent double exponential fits to the decays of the transients. *B*, Median decays (black lines) in spines and dendrites (large and small amplitude transient, respectively, n = 140). As in Fig. 1*D*, the coloured lines represent decays simulated with a kinetic model that excluded (red lines, *left*) or included (green lines, *right*) diffusional coupling between spine and dendrite. Parameters were kept as in the wild-type (WT), except that PV has been omitted from the simulation. The insets show the integrated differences between spineous data and simulations. Note that the model failed to describe the spineous decay in the absence of diffusional coupling, which is consistent with the minor contribution of PV to buffered Ca^{2+} diffusion observed in WT. *C*, as in *A* but from a mouse line that lacked both PV and calbindin ($PV/CB^{-/-}$). *D*, as in *B* but for the $PV/CB^{-/-}$ data (n = 134). All parameters were kept as in the $PV^{-/-}$ except for the removal of CB from the simulation, the alter spine morphology (Ref. 10), and an approximately two-fold increased maximum pump velocity. Note that in $PV/CB^{-/-}$ recordings, the contribution of buffered diffusion was strongly reduced for the following reasons: first, PV and CB, which accounted for ~40% of the transport in the wild type, were absent; second, $PV/CB^{-/-}$ spines show a drastically altered morphology (including longer spine necks, see Supp. Table 1); third, due to the absence of the relatively slow CaBPs CB and PV, the Ca^{2+} transients show a rapid decay that reduces the effective time window for diffusional exchange between spine and dendrite.

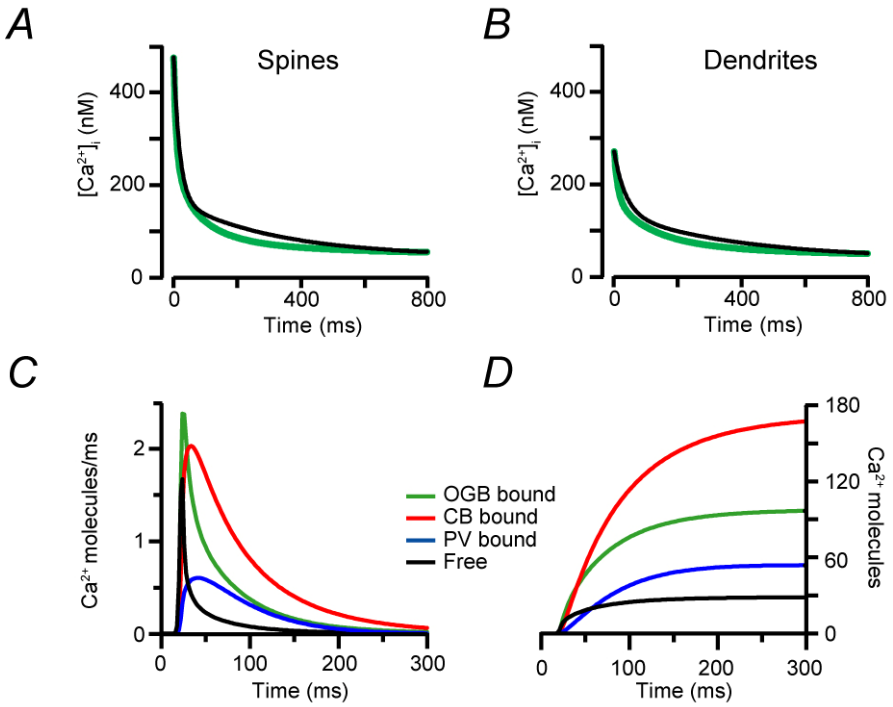

Supp. Fig. 2. Simulation of Ca^{2+} kinetics recorded at a low indicator concentration

A, Median decay kinetics in spines recorded at a dye concentration of ~40 µM (black; n = 40). The green line represents a decay simulated with the kinetic model with diffusional coupling between spine and dendrite. All parameters but the dye concentration were kept as in the WT simulation. Note that although the overlap between fit and data is not as good as in Fig. 1 and Supp. Fig. 1, characteristic features are well reproduced: the decay is more rapid than with high dye concentration while the amplitude remained almost constant. *B*, Same as in *A* but for the dendrite. *C*, Diffusional flux of free and buffer-bound Ca^{2+} across the spine neck for the simulations in *A* and *B*. *D*, Temporal integral of the diffusion flux.

Supplemental Methods

The kinetic, two-compartment model

The Ca^{2+} current (I_{Ca}) during the CF-mediated complex spike (Fig. 1 and 2*A*) and during VOCC/iGluR-mediated spine responses (Fig. 2*B*,*C*, 4*B*, S1 and S2) was represented by a Gaussian function adjusted to the time course of the measured complex spike.

$$I_{Ca} = I_0 \, 10^{-\left(\frac{t-t_0}{\sigma}\right)^2} \tag{3}$$

(Note that Eqs. 1 and 2 are to be found in the main text)

I_0 denotes the maximal amplitude of the current which is reached at t_0 and σ is the width of the function. The mGluR-mediated spineous Ca^{2+} increase (Fig. 3 and 4) was represented by an alpha-function that allowed for separate adjustment of the time constants τ of the rising and the decay phase.

$$I_{Ca} = I_0 \left(e^{-\left(\frac{t-t_0}{\tau_{decay}}\right)} - e^{-\left(\frac{t-t_0}{\tau_{rise}}\right)} \right) \tag{4}$$

The increase in $[Ca^{2+}]_i$ caused by the Ca^{2+} influx is given by

$$\left(\frac{d[Ca^{2+}]}{dt}\right)_{influx} = \frac{A \, I_{Ca}}{2 \, F \, V} \tag{5}$$

where A is the surface of the spine or dendrite, respectively, F is Faraday's constant, and V the volume of the compartment. Ca^{2+} binding to OGB, CaM, CB, and PV was simulated assuming second order kinetics for all reactions. The four binding sites of CB and the two binding sites of PV were simulated as individual reaction partners, neglecting possible cooperativity. For Ca^{2+} binding to CaM only the rate-limiting binding of the first Ca^{2+} ion was considered. Under these assumptions, the rate of change in $[Ca^{2+}]_i$ due to binding of Ca^{2+} to the j-th binding site (BS_j) is given by

$$\left(\frac{d[Ca^{2+}]}{dt}\right)_{buffer,j} = -k_{on,j}[Ca^{2+}][BS_j] + k_{off,j}[CaBS_j] \quad , \qquad \begin{matrix} j = 1 \text{ for OGB} \\ j = 2-5 \text{ for CB} \\ j = 6,7 \text{ for PV} \\ j = 8 \text{ for CaM} \end{matrix} \qquad (6)$$

For OGB, CB, and CaM the following relationship between free ($[BS]_j$) and Ca^{2+}-bound binding sites ($[CaBS]_j$) applies:

$$\left(\frac{d[BS_j]}{dt}\right) = -\left(\frac{d[CaBS_j]}{dt}\right) \quad , \qquad j = 1-5, 8 \qquad (7)$$

For PV the situation is complicated by its medium affinity for Mg^{2+} which significantly affects its Ca^{2+}-binding kinetics. The change in the occupancy of PV's binding sites is given by

$$\left(\frac{d[BS_j]}{dt}\right) = -\left(\frac{d[CaBS_j]}{dt}\right) - \left(\frac{d[MgBS_j]}{dt}\right) \quad , \qquad j = 6,7 \qquad (8)$$

and

$$\left(\frac{d[MgBS_j]}{dt}\right) = k_{on,j,Mg}[Mg^{2+}][BS_j] - k_{off,j,Mg}[MgBS_j] \quad , \qquad j = 6,7 \qquad (9)$$

The intracellular Mg^{2+} concentration was kept constant at 590 µM, a value calculated for our pipette solution using WinMaxC 2.1 software (http://www.stanford.edu/~cpatton/maxc.html). The starting conditions were calculated from chemical equilibrium at $[Ca^{2+}]_{rest}$ of 45 nM. A single surface-based Ca^{2+} extrusion mechanism was simulated assuming Michaelis-Menten kinetics (1):

$$\left(\frac{d[Ca^{2+}]}{dt}\right)_{pump} = -v_{max}\frac{A}{V}\left(\frac{[Ca^{2+}]}{[Ca^{2+}] + K_M}\right) \qquad (10)$$

where K_M is the Michaelis-Menten constant and v_{max} the maximal pump velocity. In order to establish the resting $[Ca^{2+}]_i$, the Ca^{2+} clearance was balanced by a leak current:

$$\left(\frac{d[Ca^{2+}]}{dt}\right)_{leak} = v_{max}\frac{A}{V}\left(\frac{[Ca^{2+}]_{rest}}{[Ca^{2+}]_{rest}+K_M}\right) \quad (11)$$

For a given molecular species X, the diffusional current J_X across the spine neck was simulated as

$$J_X = D_X \frac{\pi r_{neck}^2}{l_{neck}}(C_{X,spine} - C_{X,dendrite}) \quad (12)$$

where D_X and C_X are the diffusion coefficient and the concentration of the diffusing species, respectively, and r_{neck} and l_{neck} are the radius and the length of the spine neck. The rate of change in the concentration of X due to diffusion follows as

$$\left(\frac{d[X]}{dt}\right)_{diffusion} = -\frac{J_X}{V_{spine}} \quad (13a)$$

for the spine and

$$\left(\frac{d[X]}{dt}\right)_{diffusion} = \frac{J_X}{V_{dendrite}} \quad (13b)$$

for the dendrite. The simulation included independent diffusion of the free binding sites of OGB, CB, PV, and CaM, of the corresponding Ca^{2+}-bound binding sites, of the Mg^{2+}-bound binding sites of PV, and of free Ca^{2+}. The time course of the total change in $[Ca^{2+}]_i$ is given by the sum of Eqs. 5 - 11 in the absence of diffusion. Diffusional coupling was implemented by adding Eqs. 12 and 13a or b.

Supplemental Table 1. Values and Parameters of the Simulation

Parameter	Value		Notes
$[Ca^{2+}]_{rest}$	45	nM	ref. (2)
$[Mg^{2+}]_i$	590	µM	calculated, held constant
Total Ca^{2+} influx			
CF signal			
Spine	~ 4,700	ions	
Dendrite	~ 35,000	ions	
VOCC/iGluR-mediated signal			
Spine	~ 4,700	ions	
mGluR-mediated signal			
Spine	~ 54,000	ions	
Extrusion			
Michaelis-Menten constant, K_M	3	µM	
Maximal pump velocity, v_{max}	30-300	pmol $cm^{-2}s^{-1}$	
Oregon Green BAPTA-1			
Effective concentration	160 or 40	µM	80% of pipette conc.
K_D	325	nM	ref. (3)
k_{off}	140	s^{-1}	ref. (4) and [a]
k_{on}	430	$\mu M^{-1}s^{-1}$	calculated
Calbindin D_{28k}			
Effective concentration	100	µM	ref. (5) and [b]
After correction for wash-out	50	µM	[c]
Binding sites (non-cooperative)	4		ref. (6)
Ratio of high- to medium-affinity binding sites	2:2		ditto
$k_{off, medium aff.}$	35.8	s^{-1}	ditto
$k_{off, high aff.}$	2.6	s^{-1}	ditto
$k_{on, medium aff.}$	43.5	$\mu M^{-1}s^{-1}$	ditto and [d]
$k_{on, high aff.}$	5.5	$\mu M^{-1}s^{-1}$	ditto
$K_{D, medium aff.}$	822	nM	calculated
$K_{D, high aff.}$	474	nM	calculated
Parvalbumin			
Effective concentration	75	µM	ref. (5)
After correction for wash-out	40	µM	[c]
Binding sites (non-cooperative)	2		ref. (7)
$k_{off,Ca}$	0.95	s^{-1}	ref. (8)
$k_{off,Mg}$	25	s^{-1}	ditto
$K_{D,Ca}$	9	nM	ditto
$K_{D,Mg}$	31	µM	ref. (7)
$k_{on,Ca}$	107	$\mu M^{-1}s^{-1}$	calculated
$k_{on,Mg}$	0.8	$\mu M^{-1}s^{-1}$	calculated

Supplemental Table 1, continued

Parameter	Value		Notes
Calmodulin			
Effective concentration	10	µM	estimated from ref. (3)
Binding sites	1		
k_{off}	2,200	s^{-1}	[e]
K_D	55	µM	ditto
k_{on}	40	$\mu M^{-1}s^{-1}$	ditto
Geometry			
Wild type and $PV^{-/-}$			
Volume of spine head	0.083	μm^3	ref. (9)
Surface area of spine head	0.9	μm^2	ditto
Radius of spine neck	0.09	µm	ditto
Length of spine neck	0.66	µm	ditto
Spine density	3.4	μm^{-1}	ref. (10)
Radius of dendritic segment	1	µm	
Length of dendritic segment	0.3	µm	calculated from spine density
$PV/CB^{-/-}$			
Volume of spine head	0.2	μm^3	estimated [f]
Surface area of spine head	1.8	μm^2	ditto
Radius of spine neck	0.1	µm	ditto
Length of spine neck	1.3	µm	ditto
Spine density	5	μm^{-1}	ref. (10)
Radius of dendritic segment	1	µm	
Length of dendritic segment	0.2	µm	calculated from spine density
Diffusional mobility			
D_{Ca}	223	μm^2s^{-1}	ref. (11)
D_{OGB}	15	μm^2s^{-1}	ref. (12) and [a]
D_{PV}	43	μm^2s^{-1}	ref. (13)
D_{CB}	20	μm^2s^{-1}	ref. (14)
D_{CaM}	21	μm^2s^{-1}	this study
Fraction of immobile CB	0.2		ref. (14)
Fraction of immobile CaM	0.2		this study

[a] Data for Calcium Green 1, an indicator dye closely related to OGB; [b] assuming that 33% of CB is occupied by Mg^{2+}; [c] assuming a ~50% washout during our whole-cell recordings; [d] assuming two-fold slower kinetics in the cytosol compared to the *in vitro* data (15); [e] Faas *et al*. (2004), Soc. Neurosci. Abstr. No 165.5; [f] calculated from the wild-type EM data based on the observation of a ~2 fold increase in volume, surface, and length in spines of $PV/CB^{-/-}$ mice (10).

1. Sala, F. & Hernández-Cruz, A. (1990) *Biophys. J.* **57,** 313-324.
2. Airaksinen, M. S., Eilers, J., Garaschuk, O., Thoenen, H., Konnerth, A. & Meyer, M. (1997) *Proc. Natl. Acad. Sci. USA* **94,** 1488-1493.
3. Schmidt, H., Stiefel, K., Racay, P., Schwaller, B. & Eilers, J. (2003) *J. Physiol. (London)* **551,** 13-32.
4. Eberhard, M. & Erne, P. (1991) *Biochem. Biophys. Res. Commun.* **180,** 209-215.
5. Kosaka, T., Kosaka, K., Nakayama, T., Hunziker, W. & Heizmann, C. W. (1993) *Exp. Brain Res.* **93,** 483-491.
6. Nägerl, U. V., Novo, D., Mody, I. & Vergara, J. L. (2000) *Biophys. J.* **79,** 3009-3018.
7. Eberhard, M. & Erne, P. (1994) *Eur. J. Biochem.* **222,** 21-26.
8. Lee, S.-H., Schwaller, B. & Neher, E. (2000) *J. Physiol. (Lond.)* **525,** 419-432.
9. Harris, K. M. & Stevens, J. K. (1988) *J. Neurosci.* **8,** 4455-4469.
10. Vecellio, M., Schwaller, B., Meyer, M., Hunziker, W. & Celio, M. R. (2000) *Eur. J. Neurosci.* **12,** 945-954.
11. Allbritton, N. L., Meyer, T. & Stryer, L. (1992) *Science* **258,** 1812-1815.
12. Holthoff, K., Tsay, D. & Yuste, R. (2002) *Neuron* **33,** 425-437.
13. Schmidt, H., Brown, E. B., Schwaller, B. & Eilers, J. (2003) *Biophys. J.* **84,** 2599-2608.
14. Schmidt, H., Schwaller, B. & Eilers, J. (2005) *Proc. Natl. Acad. Sci. USA* **102,** 5850-5855.
15. Berggård, T., Miron, S., Önnerfjord, P., Thulin, E., Åkerfeldt, K. S., Enghild, J. J., Akke, M. & Linse, S. (2002) *J. Biol. Chem.* **277,** 16662-72.